108665

U.S. Department of Transportation

National Highway Traffic Safety Administration

Memorandum

Subject: ACTION: Submittal of Technical Paper, "Effects of Upper Neck Joint Stiffness on Measured Moments in the Hybrid III Dummy During Airbag Loading" to Docket No. NHTSA-2000-7013-46

Date:

Reply to Attn. of:

From: Rolf Eppinger
Chief, National Transportation Biomechanics Research Center

To: Raymond P. Owings, Ph.D.
Associate Administrator for Research and Development

The Docket
THRU: Frank Seales, Jr.
Office of Chief Counsel

Attached are two copies of the technical paper, "Effects of Upper Neck Joint Stiffness on Measured Moments in the Hybrid III Dummy During Airbag Loading." A parametric analysis of upper neck joint stiffness was performed using the MADYMO occupant kinematics software to determine how the rotational and axial neck stiffnesses of the Hybrid III dummy affect the measured moments, forces, and kinematics during airbag loading.

2 Attachments

CONCUR: ✓ Lance Bjus Mat

NONCONCUR: _____

DATE: 9-11-00

#

Get it together!
SAFETY BELTS SAVE LIVES

EFFECTS OF UPPER NECK JOINT STIFFNESS ON MEASURED MOMENTS IN THE HYBRID III DUMMY DURING AIRBAG LOADING

Roger W. Nightingale, Ph.D., †Michael Kleinberger, Ph.D.,
Barry S. Myers, M.D., Ph.D.

Duke University, Department of Biomedical Engineering
Duke University, Division of Orthopaedic Surgery
† *Johns Hopkins, Applied Physics Laboratories*

August 25, 2000

1 INTRODUCTION

This study was designed to determine how the rotational and axial neck stiffnesses of the IIybrid III dummy affect the measured moments, forces, and kinematics during airbag loading. A parametric analysis of upper neck joint stiffness was performed using the MADYMO occupant kinematics software. This study compares the responses of the standard TNO MADYMO two-pivot neck with versions which are modified to simulate more realistic axial stiffness and rotational stiffness. Axial stiffness data for the modified necks were taken from the literature. Rotational stiffness data for the modified necks was derived from flexibility testing of cadaveric head/neck specimens. Results for more sophisticated MADYMO necks, such as the TNO 5 joint Hybrid III neck and the de Jager Global HUMAN Head-Neck Model, are also presented.

2 METHODS

2.1 FLEXIBILITY OF O-C1

Experiments were conducted on ten unembalmed male human head and cervical spine preparations with an age range of 53 to 80 years (66±8.2). Stainless steel pins (4-8 cm long) terminating in photo-absorptive spheres (8 mm diameter) were inserted into the left anterior vertebral body, the right anterior vertebral body, the lateral mass, and the spinous process of C2-T1. The spheres served as markers for digitization.

The sagittal plane bending responses of each cervical spine were tested in a load frame designed to apply pure moments (Panjabi et al., 1988, Yamamoto et al., 1989, Oda et al., 1991). The specimen was turned upside-down and mounted in the load frame (Figure 1). A moment application apparatus was attached to the T1 vertebra, and a counterweighting device opposed the combined weight of the moment application apparatus, and the weight of the average cervical spine. A three-axis load cell (GSE Inc Model T-11449-A, Farmington Hills, MI) beneath the specimen measured the reactions and verified that the moment remained pure.

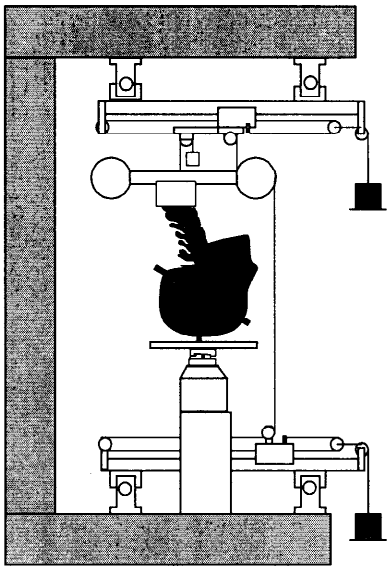

FIGURE 1: A schematic of the bending flexibility test frame. Cervical spines were tested in flexion, extension, lateral bending and torsion. Bending moments were kept pure using 2-D translation stages supporting the force couple.

Two CCD cameras (Kodak EM-2, Charlotte, NC) were oriented at approximately 60° to visualize the three-dimensional positions of each vertebra following each load step. Pure moments up to 1.5 N-m (flexion) and up to –1.5 N-m (extension) were applied in 0.1 N-m increments by hanging masses on two holders attached to the moment application apparatus by a system of nylon string, pulleys, rollers, and bearings. At each load step, the specimen was allowed to creep for 50 seconds (McElhaney et al., 1983) and then imaged by both cameras. The three-dimensional positions of the pins were reconstructed from the planar images by direct linear transformation (DLT) (Veldpaus et al., 1988, Woltring, 1980). Cardan angles were calculated using the algorithm developed by Woltring (1991) (mean error ±0.062 degrees).

Due to difficulties in visualizing C1 during testing, it was only possible to measure motion between the occiput and C2. To estimate the flexibility of the O–C1 and C1–C2 motion segments, 70 percent of the flexion-extension flexibility was attributed to the O–C1 motion segment and the remaining 30 percent was attributed to the C1–C2 motion segment (Fielding, 1957, Goel et al., 1988, Oda et al., 1992).

In order to generate joint flexibilities for the MADYMO model, it was necessary to average the flexion-extension responses of each motion segment. The flexion-extension responses were fit using the function:

$$\theta = \frac{1}{B} \ln\left(\frac{M}{A} + 1\right), \tag{1}$$

where A and B are constant coefficients and M is the applied moment (Fung, 1972, Simon et al., 1984). Because of uncertainty in the reference position for each cervical spine, these functions were shifted along the vertical axis using a least squares minimization routine so that the proportion of the total range of motion in flexion relative to the total range of motion in extension was the same for all motion segments at a given level. These analytical functions were then averaged from 0 to 1.5 N-m at 0.1 N-m intervals. The flexibility tests resulted in moment-angle relationships for the C7-T1 through C3 motion segments and the O–C2 complex (Appendix A) (Camacho et al., 1997).

2.2 MADYMO MODELING

Simulations were conducted using the MADYMO software, and the Hybrid III dummy databases supplied with the software distribution. These databases were created and validated by TNO using data from belted sled tests. Three different MADYMO Hybrid III necks were used in this study. The first is the standard TNO dummy model (**d3hyb350.dat**) in which the neck consists of a 2 pivot segment which links the head and upper torso using flexion-torsion restraints. The second is a modification of **d3hyb350.dat**, released as **d3hyb350.n5j.dat**, which incorporates a 5 joint neck model. The third database uses a "global HUMAN head-neck model" (**d3hunkgl.dat**) which was developed by de Jager (de Jager, 1996) and is heretofore referred to as the de Jager model.

2.2.1 Airbag Characteristics

The airbag characteristics used in these simulations were the ones supplied by TNO in their software distribution (**affoldbag.dat**). Prior to the simulations, the TNO airbag characteristics were compared with those from tank test data for the vehicles tested by VRTC. Based on both peak pressure and rise time, the TNO airbag was considered more aggressive than any of the bags tested. On this basis, we decided to use the TNO airbag model for the parametric analysis of neck stiffness, keeping in mind that the results are indicative of aggressive airbag loading.

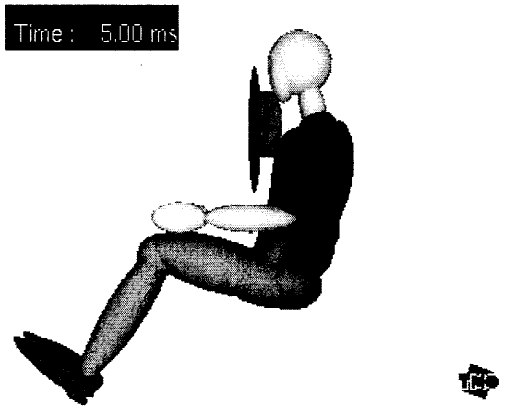

FIGURE 2: The initial position of the dummy relative to the airbag for all simulations.

2.2.2 Verification

The standard MADYMO Hybrid III model was verified for out-of-position air bag deployment simulations by comparing the model output with experimental Hybrid III test data from NHTSA's Vehicle Research and Test Center (VRTC). The MADYMO 50th percentile Hybrid III dummy was positioned in front of an airbag in the driver out-of-position ISO position 1 used by VRTC in their static deployment tests with 5th percentile female dummies (Figure 2). In the simulations, the dummy was kept in a normally seated position while the steering wheel and airbag module were repositioned with respect to the dummy's head and neck. In order to minimize the number of variables, there was no seat model in the simulations. In addition, the acceleration of gravity was not included. The response of the model was verified by comparing the model output with the data from the following four VRTC tests: 3345 (D3960001), 3348 (D3960004), 3349 (D3960005), and 3351 (D3960007). The male dummy model was used in the simulations because it has been more rigorously validated; however, its response was compared to the 5th percentile female model (**d3hyb305.dat**). Results for this comparison are presented in Figure B.2.

2.2.3 Analysis of Neck Stiffness

The effects of rotational and axial stiffness were examined by comparing the results from four versions of the standard, two-pivot MADYMO model (**d3hyb350.dat**). The first is the standard TNO Hybrid III model with the original joint stiffnesses (TNO1). The

second is a Hybrid III model which was modified to include an axial neck stiffness of 58.5 kN/m in tension (Yoganandan et al., 1996) (note: the axial neck stiffness is infinite in the standard MADYMO model). This was accomplished by dividing the single neck body into 2 bodies connected by a translational joint. The second model is designated as TNO1AX. The third model is the same as the second with the addition of the rotational stiffness of O–C1 from the cadaver testing (TNO1AXROT). The fourth is the Hybrid III model with the rotational stiffness of O–C1 from the flexibility experiments (TNO1ROT). These are all summarized in Table 1. All the reaction data was filtered using the SAE J211 CFC1000.

TABLE 1: Matrix of Simulations

Test	Upper Neck Joint Model	
	Axial	Rotational
TNO1	TNO Hybrid III	TNO Hybrid III
TNO1AX	Cadaver skull T3	TNO Hybrid III
TNO1AXROT	Cadaver skull–T3	Cadaver O–C1
TNO1ROT	TNO Hybrid III	Cadaver O–C1

2.2.4 Advanced Neck Models

The TNO 5 joint neck model and the de Jager model were also tested for out-of-position occupant airbag deployments. Implementation of the 5 joint model was relatively straightforward; however, the de Jager model posed some problems. First, it was necessary to add a bracket joint above O-C1 and at the centroid of the upper neck load cell (in the head coordinate system) in order to create a location for the measurement of neck reactions. Second, the geometry of the de Jager neck model is not the same as the 50th percentile Hybrid III male neck, particularly in the axial dimension. The longer neck of the de Jager model resulted in a higher head position relative to the torso and the airbag. In order to keep the initial position as close as possible to the Hybrid III models, the head and neck were lowered by moving the T1 joint downwards 1.5 cm relative to the upper torso. The final complicating factor was the location of the center of rotation of the O-C1 joint. In the human, the center of rotation is well above the condyles, and therefore, well above the pin joint in the Hybrid III neck. As a result, it was impossible to place the upper neck

load cell bracket joint in the appropriate location relative to both the O-C1 joint and the head. It was elected to place the bracket joint directly on the O-C1 joint since this is the location of greatest clinical interest. A parametric analysis of load cell placement was also performed.

3 RESULTS AND DISCUSSION

3.1 MODEL VERIFICATION

The MADYMO model of the 50th percentile Hybrid III dummy (TNO1) gave qualitatively similar responses when compared to the VRTC tests (Appendix B). The most significant reactions in the VRTC tests are the neck shear force, the tensile force, and the extension moment. The MADYMO simulations resulted in peaks loads that were a little higher than the VRTC tests, and the impulse durations were a little shorter than in the VRTC tests. The differences between the simulations and the VRTC tests can be attributed to the greater stiffness of the MADYMO models (most of the segments have no axial compliance), and to the fact that the MADYMO databases were validated for non-contact decelerations. Another difference is the use of the more rigorously validated 50th percentile male model rather than the 5th percentile female. Despite these differences, the simulations are sufficiently similar to the VRTC tests to allow a credible analysis of the comparative effects of neck stiffness on the reactions at the upper neck joint.

TABLE 2: Peak Reactions and Airbag Parameters

	Upper Neck Reactions				Airbag	
Test	Shear (N)	Tension (N)	Moment (N-m)	HIC	Press. (kN/m^2)	Vol. (cm^3)
TNO1	2787	4744	-173	202	421	32500
TNO1AX	2653	3503	-152	283	432	36500
TNO1AXROT	2769	3717	-72	363	430	39100
TNO1ROT	4105	4599	-123	387	425	32700
TNON5J	2738	4650	-192	259	466	33600
de Jager	3501	4346	-115	781	459	37100

3.2 STIFFNESS ANALYSIS

The results of the simulations are summarized in Table 2 and plots of all the reaction data are compiled in Appendix C (Figure C.1). The addition of axial compliance to the neck (TNO1AX) resulted in a significant drop in the tensile neck force. However, the shear force and the peak extension moment were relatively unchanged. The addition of rotational compliance (TNO1ROT) resulted in an increase in the peak shear force and a decrease in the extension moment. The addition of both axial and rotational compliance resulted in a decrease of the peak tension and a dramatic decrease of the peak extension moment. As the compliance of the neck was increased, the HIC values also increased because the head was increasingly less constrained. Therefore, the simulation with the most flexible neck (TNO1AXROT) was also the simulation with the largest HIC. However, none of the simulations generated HICs greater than 1000.

3.3 AIRBAG KINEMATICS

The kinematics for all the simulations are compiled in Appendix D. It is immediately evident from the kinematics that the stiffness of the neck influences the deployment of the airbag; therefore, the loading conditions on the dummy were not identical for all four simulations (Figure 3). This can also be seen in the airbag pressure and volume peaks (Table 2). This means that relatively small differences in peak values should be interpreted with caution. Also note that the force histories for the simulations *without* axial neck compliance (TNO1 and TNO1ROT) have more high frequency components than those with axial compliance. This also influences the peak values. In fact, this would be a very good argument for not using the default Hybrid III neck for these types of studies.

In all the simulations, the airbag eventually deployed either to the left or to the right of the head and neck. This asymmetry was not evident until approximately 18 milliseconds after deployment was initiated. Since most of the peak forces and moments occurred at approximately 20 milliseconds, the asymmetric deployment probably had little effect on the peak values in these simulations.

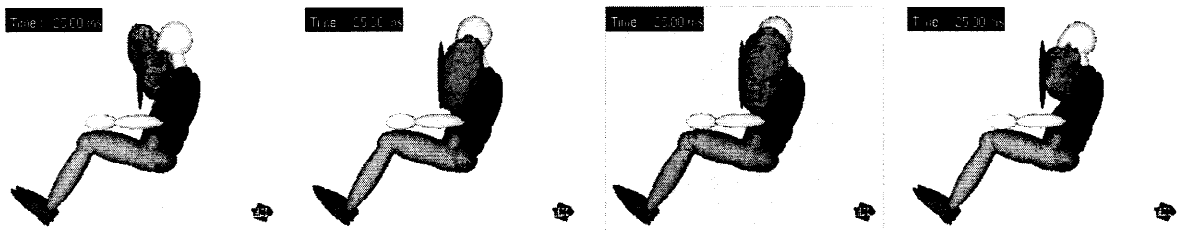

TNO1 TNO1AX TNO1AXROT TNO1ROT

FIGURE 3: Images of all four simulations at 25 milliseconds, showing the effects of neck compliance on the deployment of the airbag.

3.4 ADVANCED NECK MODELS

The results for the advance models are summarized in Table 2 and the plots of the reaction data are shown in Figure C.2. The responses of the standard neck and the 5 joint neck were not appreciably different; however, the impulse duration for the 5 body neck was considerably longer (Figure C.2). This is most likely due to the symmetric deployment of the airbag in the simulation using the 5 joint model. The de Jager model had a 57 percent decrease in extension moment when compared to the standard model, however, the peak tensile load was not appreciably different and the peak shear load was greater.

The results from the analysis of load cell position in the de Jager model are shown in Figure C.3. Although there are some differences in peak loads due to airbag deployment, there is an expected increase in moment with increasing eccentricity. In the case of maximum eccentricity (15 mm), the peak moment was -137 N-m as compared to -115 N-m (a 20 percent increase).

3.5 SUMMARY

This study demonstrates how changes in the upper neck joint of the Hybrid III dummy can affect the reactions. The standard TNO MADYMO dummy model was modified to simulate the axial and rotational stiffnesses of *the ligamentous human cervical spine*. Since the effects of neck musculature were not included, these simulations represent an extremum in neck compliance. Decreasing the axial stiffness of the neck in these simulations

did not have a profound effect on the neck reactions at the upper cervical joint. In contrast, decreasing the rotational stiffness had a dramatic effect on the extension moment. The combination of decreased axial stiffness and decreased rotational stiffness reduced the peak extension moment by a factor of 3.2. These decreases in neck moments were accompanied by increases in the HIC values.

There was no significant difference in performance between the advanced, 5-joint TNO Hybrid III neck model and the standard 2-joint model. The de Jager model, which was based on flexibility data, had significantly lower moments than the Hybrid III models. However, the de Jager model generated significantly larger moments than the standard model with the modified O-C1 joint.

REFERENCES

Camacho, D. L. A., Nightingale, R. W., Robinette, J. J., Vanguri, S. K., Coates, D. J., and Myers, B. S. (1997). Experimental flexibility measurements for the development of a computational head-neck model validated for near-vertex head impact. In *41st Stapp Car Crash Conference Proceedings*, number 973345, pages 473–486. Society of Automotive Engineers.

de Jager, M. (1996). *Mathematical Head-Neck Models for Acceleration Impacts.* PhD thesis, Eindhoven University of Technology, Faculty of Mechanical Engineering.

Fielding, J. W. (1957). Cineroentgenography of the normal cervical spine. *Journal of Bone and Joint Surgery*, **39-A**(6):1280–1288.

Fung, Y. C. B. (1972). Stress-strain-history relations of soft tissues in simple elongation. In Fung, Y. C. B., Perrone, N., and Anliker, M., editors, *Biomechanics: Its Foundations and Objectives*, pages 181–208. Prentice-Hall.

Goel, V. K., Clark, C. R., Gallaes, K., and Liu, Y. K. (1988). Moment-rotation relationships of the ligamentous occipito-atlanto-axial complex. *Journal of Biomechanics*, **21**(8):673–680.

McElhaney, J. H., Paver, J. G., McCrackin, H. J., and Maxwell, G. M. (1983). Cervical spine compression responses. *Proc. 27th Stapp Car Crash Conference*, (831615):163–177.

Oda, T., Panjabi, M., and Crisco, J. J. (1991). Three-dimensional translational movements of the upper cervical spine. *Journal of Spinal Disorders*, **4**(4):411–419.

Oda, T., Panjabi, M., Crisco, J. J., Bueff, H. U., Grob, D., and Dvorak, J. (1992). Role of the tectorial membrane in the stability of the upper cervical spine. *Clinical Biomechanics*, **7**:201–207.

Panjabi, M. M., Dvorak, J., Duranceau, J., Yamamoto, I., Gerber, M., Rauschning, W., and Bueff, H. U. (1988). Three-dimensional movements of the upper cervical spine. *Spine*, **13**(7):726–730.

Simon, B. R., Coats, R. S., and Woo, S. L.-Y. (1984). Relaxation and creep quasilinear viscoelastic models for normal articular cartilage. *Journal of Biomechanical Engineering*, **106**:159–164.

Veldpaus, F. E., Woltring, H. J., and Dortmans, L. J. G. M. (1988). Planar control in multi-camera calibration for 3-d gait studies. *Journal of Biomechanics*, **21**(1):45–54.

Woltring, H. J. (1980). Planar control in multi-camera calibration for 3-d gait studies. *Journal of Biomechanics*, **13**(2):39–48.

Woltring, H. J. (1991). Representation and calculation of 3-d joint movement. *Human Movement Science*, **10**:603–616.

Yamamoto, I., Panjabi, M., Crisco, J., and Oxland, T. (1989). Three-dimensional movements of the whole lumbar spine and lumbosacral joint. *Spine*, **14**(11):1256–1260.

Yoganandan, N., Pintar, F. A., Maiman, D. J., Cusick, J. F., Jr, A. S., and Walsh, P. R. (1996). Human head-neck biomechanics under axial tension. *Med Eng Phys*, **18**(4):289–294.

APPENDIX A

HUMAN CERVICAL SPINE FLEXIBILITY

The averaged flexibility data for each motion segment in flexion and extension are shown below. The following is a list of all the motion segments for which data is reported and the sample size which serves as the basis for the averaging: O–C2 (n=5), C2–C3 (n=7), C3–C4 (n=9), C4–C5 (n=8), C5–C6 (n=7), C6–C7 (n=8), and C7–T1 (n=9). The data in each graph shows the average and standard deviation for all the motion segment functions at increments of 0.1 N-m. This average flexibility data can be fit using equation (2) and the coefficients given in the figure captions ($r > 0.999$ for all fits).

$$\theta = \frac{1}{B} \ln\left(\frac{M}{A} + 1\right), \qquad (2)$$

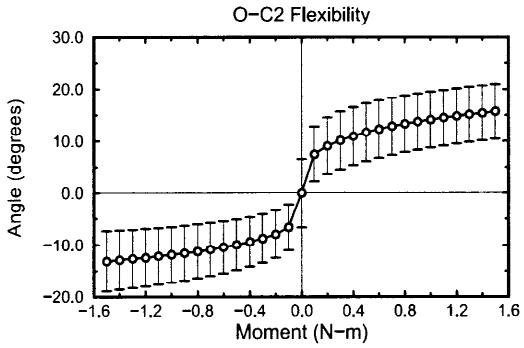

(flexion A=0.0135 B=0.3052)
(extension A=–0.0095 B=–0.3937)

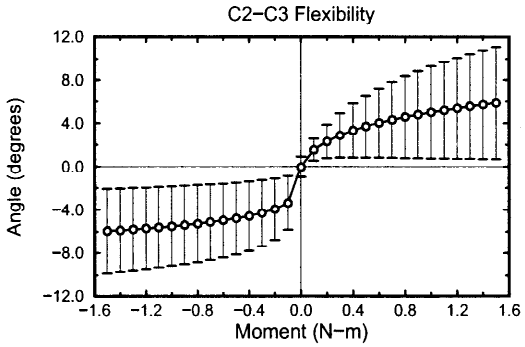

(flexion A=0.1029 B=0.4714)
(extension A=–0.0037 B=–1.0137)

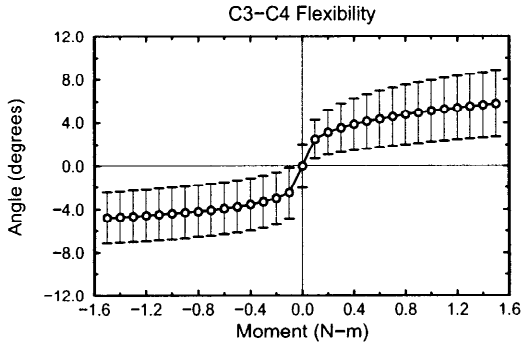

(flexion A=0.0218 B=0.7503)
(extension A=–0.0068 B=–1.1416)

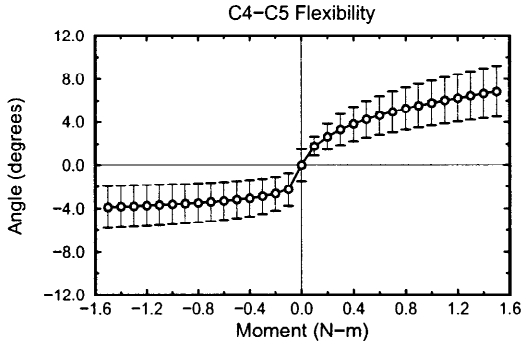

(flexion A=0.1130 B=0.3929)
(extension A=–0.0027 B=–1.6410)

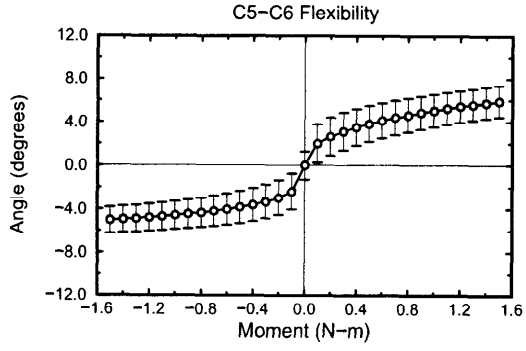

(flexion A=0.0618 B=0.5587)
(extension A=–0.0126 B=–0.9581)

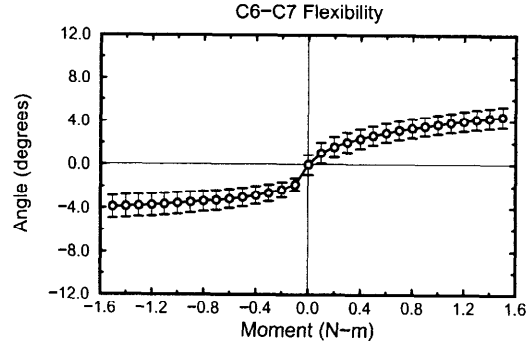

(flexion A=0.1406 B=0.5607)
(extension A=–0.0125 B=–1.2366)

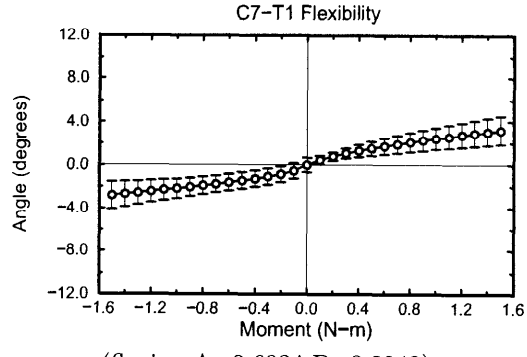

(flexion A=0.6084 B=0.3949)
(extension A=–0.3105 B=–0.6489)

APPENDIX B

VRTC OUT-OF-POSITION AIRBAG TESTS

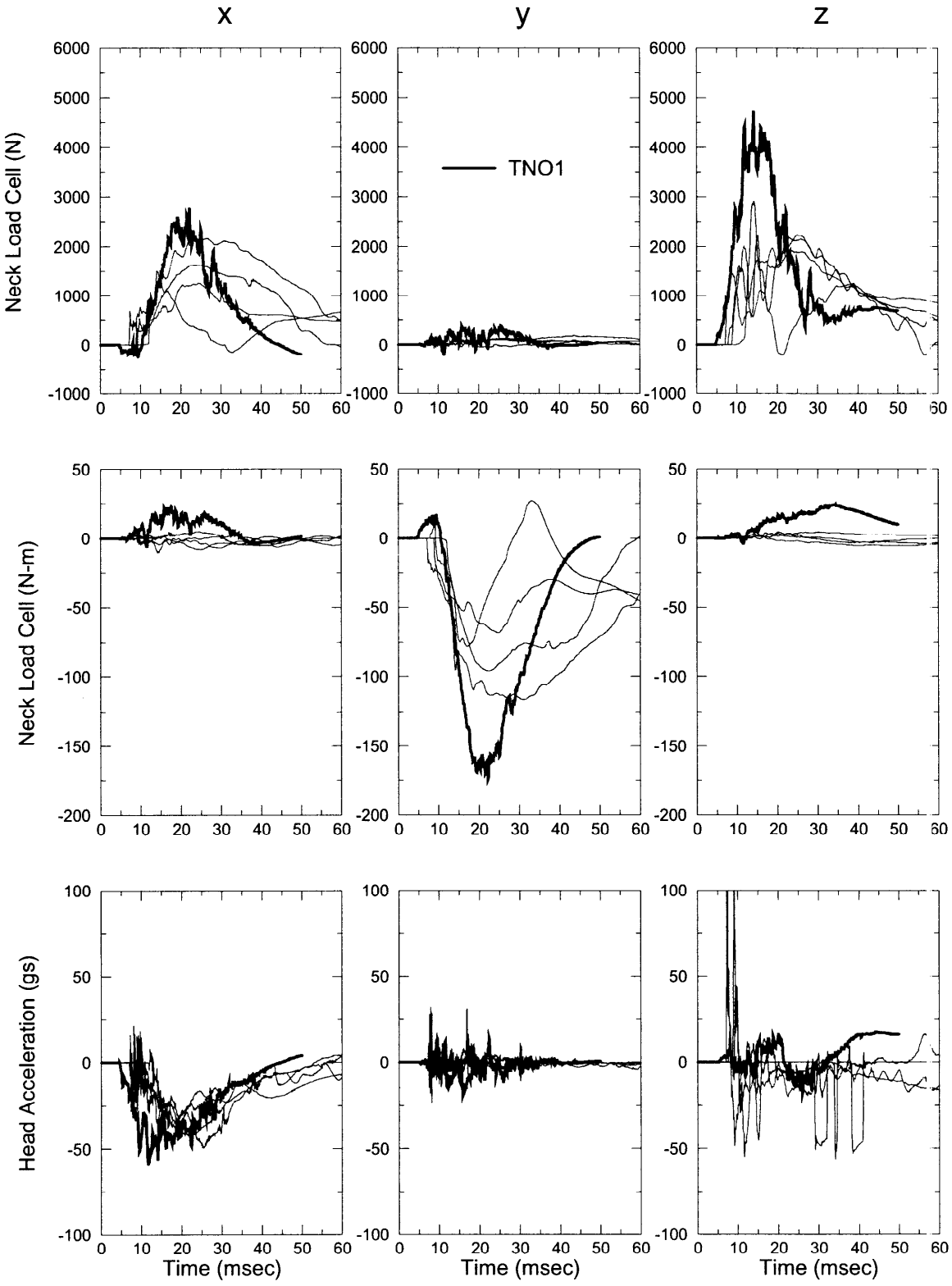

FIGURE B.1 The neck loads and head accelerations for the out-of-position 50th percentile male MADYMO model. The model results (TNO1) are in bold. The model compares favorably with the results from four VRTC tests.

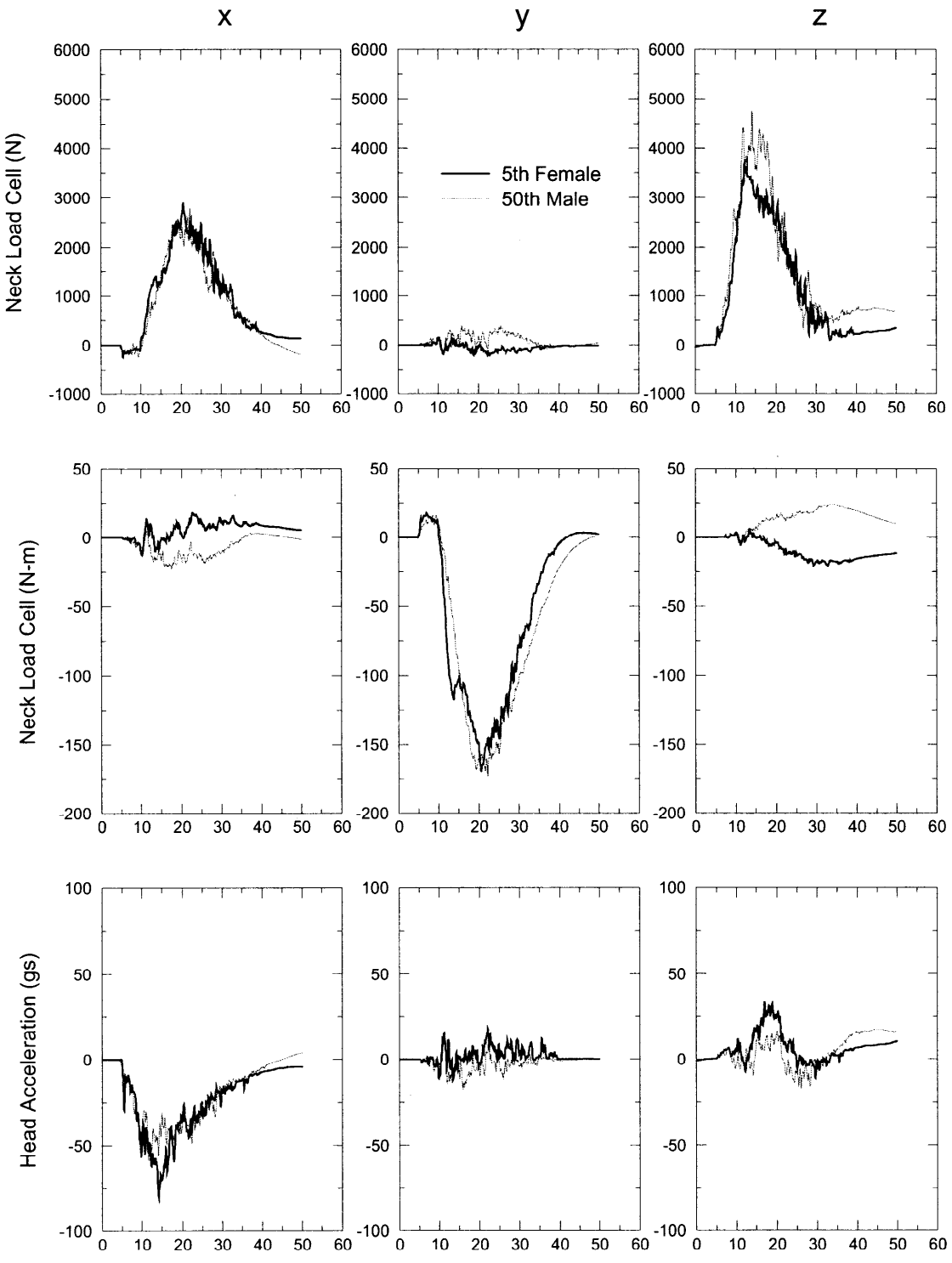

FIGURE B.2 A comparison of the 50th percentile male model and the 5th percentile female model.

APPENDIX C

SIMULATION RESULTS: REACTIONS

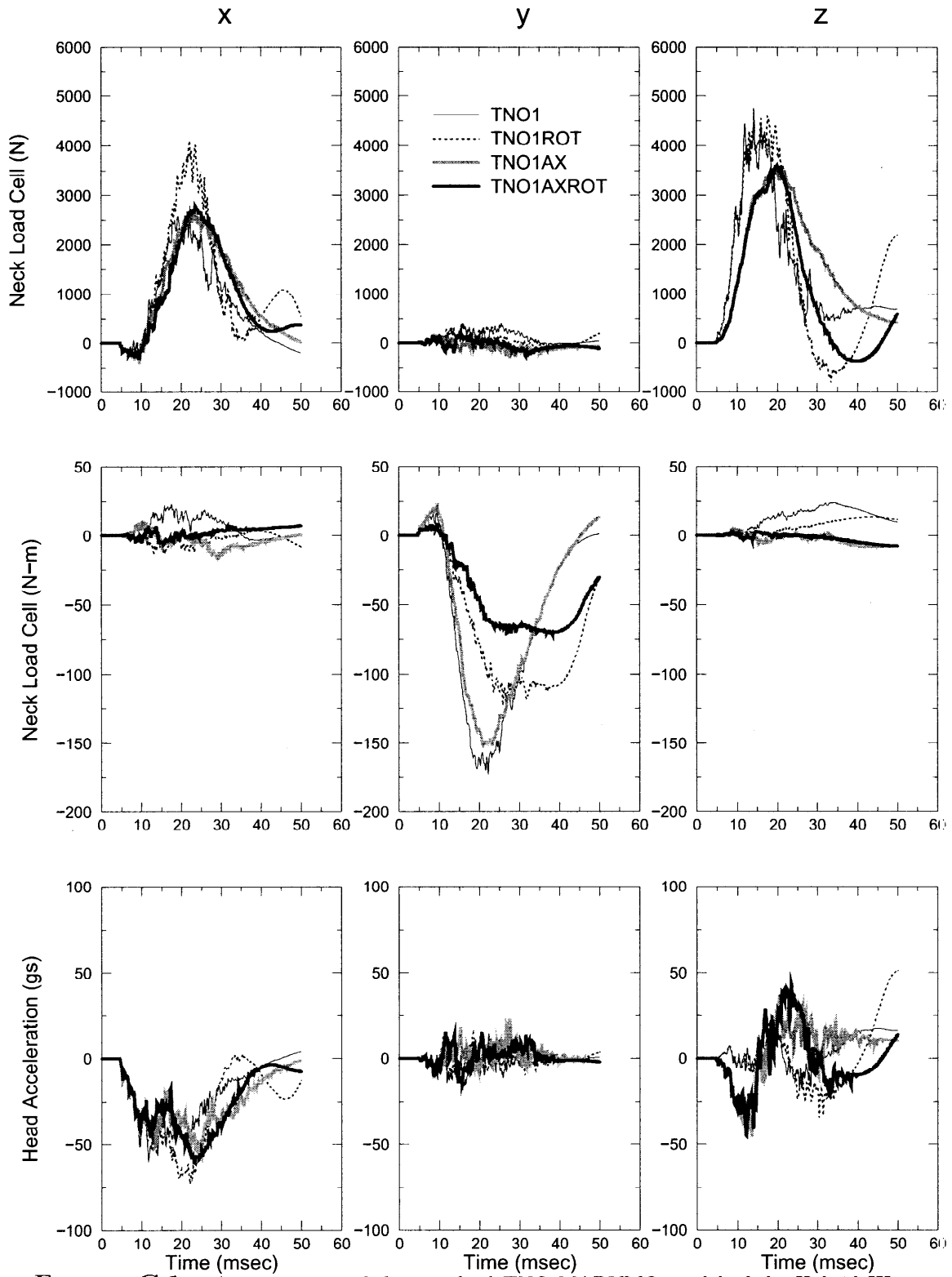

FIGURE C.1 A comparison of the standard TNO MADYMO model of the Hybrid III neck (TNO1) with the three modifications. Peak moments were decreased by the addition of the cadaver based flexibility at O-C1. Peak tensile loads were decreased by the addition of axial compliance.

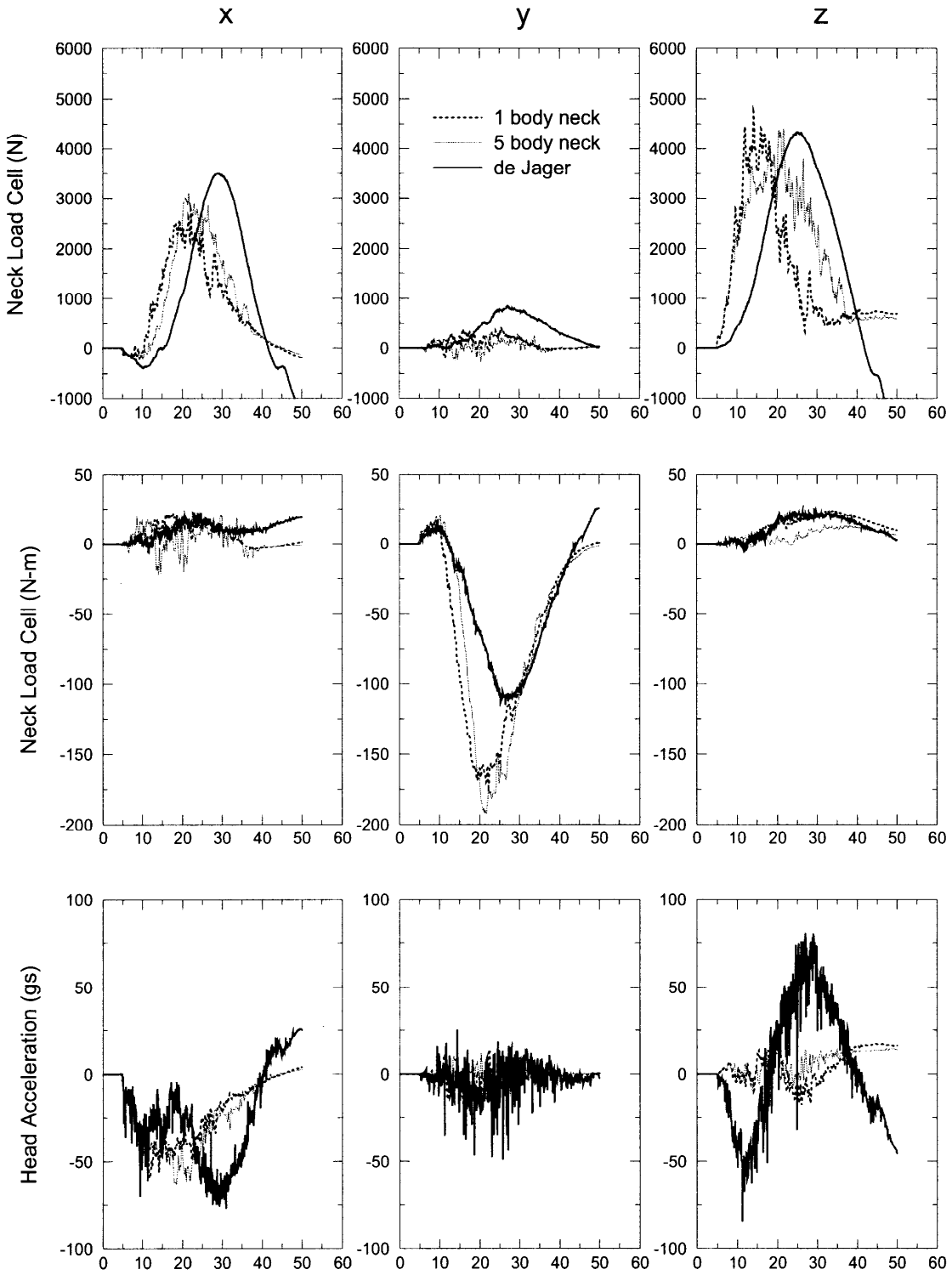

FIGURE C.2 A comparison of the three neck models available from TNO.

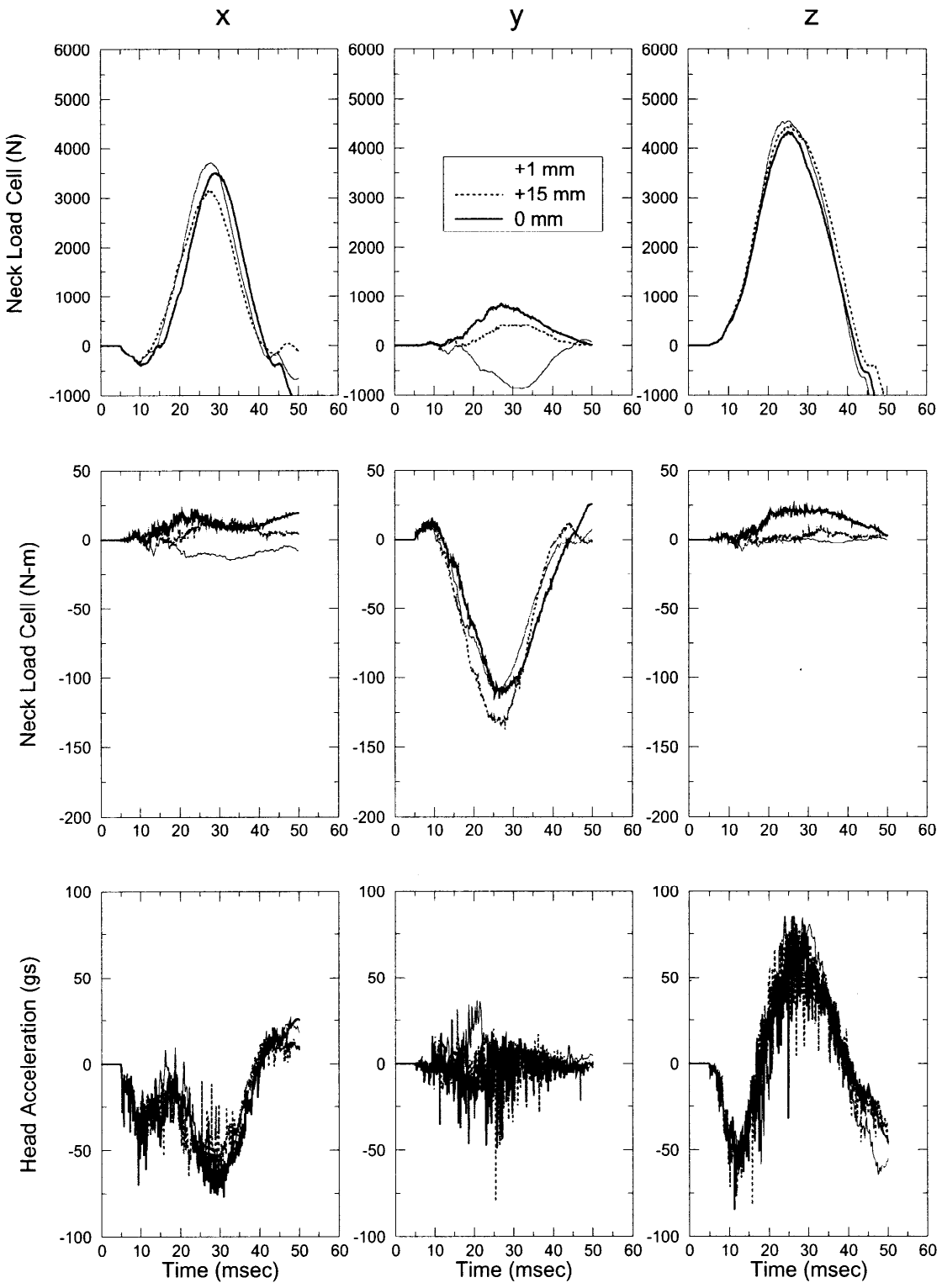

FIGURE C.3 A parametric analysis of the effect of load cell location on the reactions at the upper load cell for the de Jager model.

APPENDIX F

SIMULATION RESULTS: KINEMATICS

MADYMO Neck (TNO1)

Modified O-C1 (TNO1ROT)

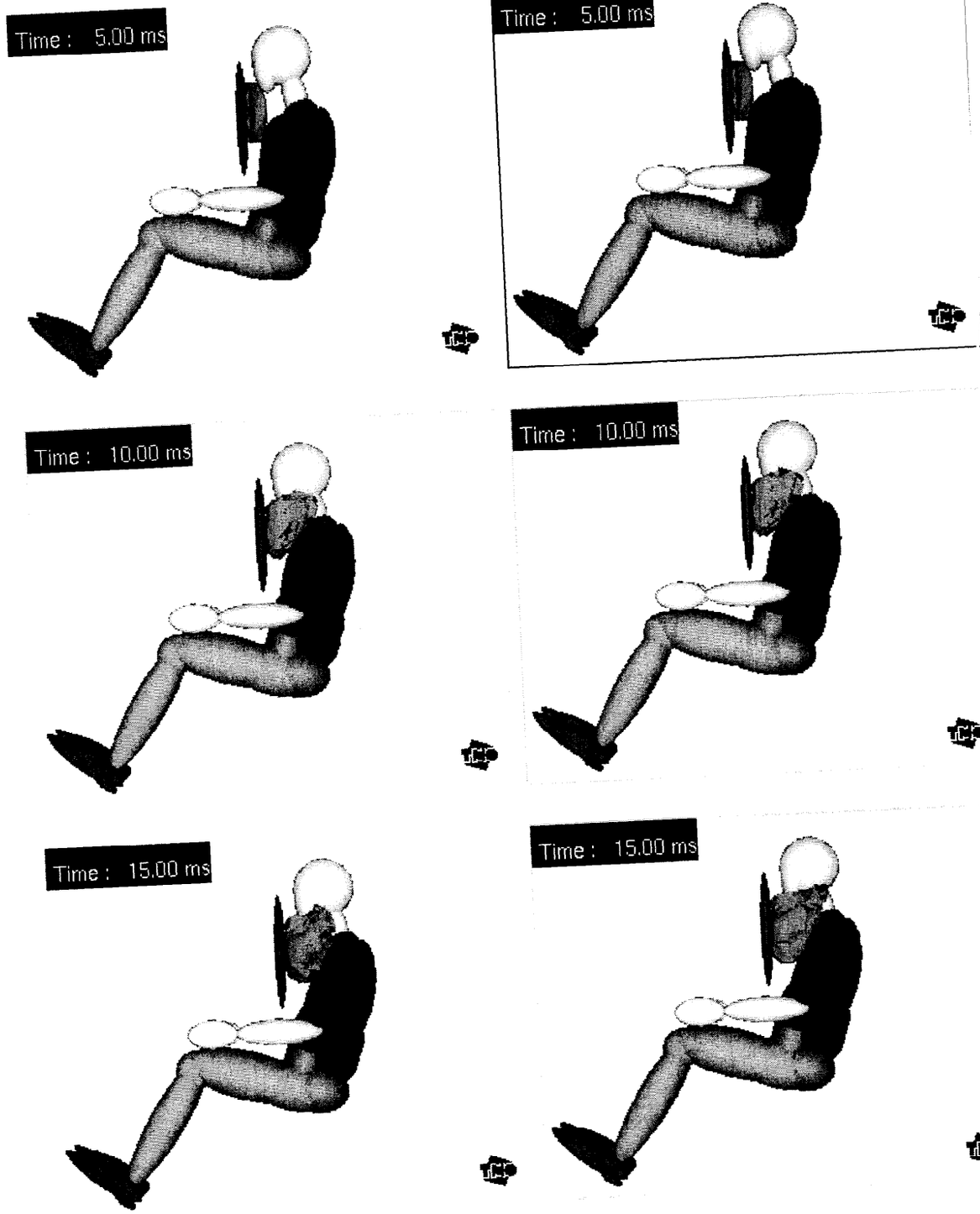

MADYMO Neck (TNO1)

Modified O-C1 (TNO1ROT)

MADYMO Neck (TNO1)

Modified O-C1 (TNO1ROT)

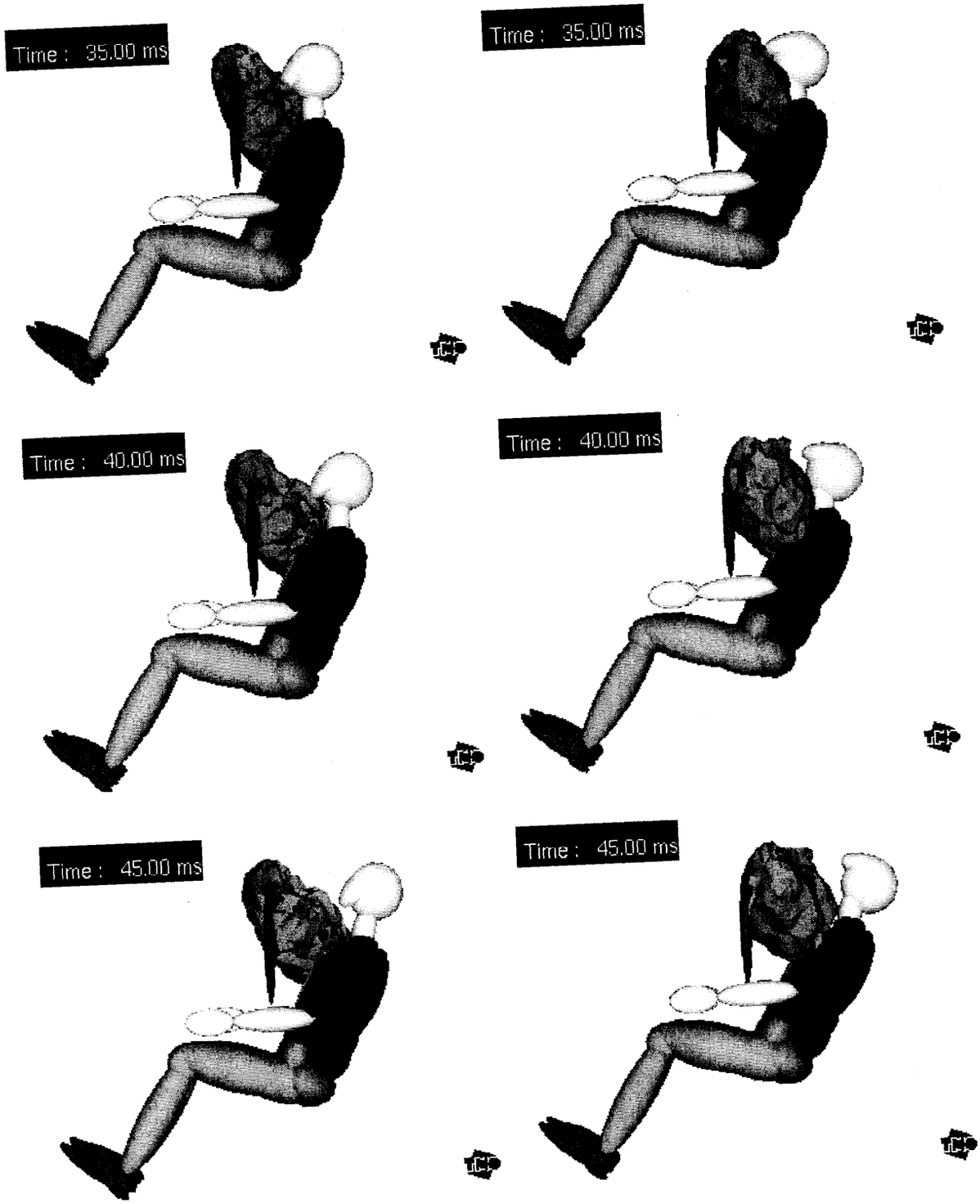

MADYMO Neck (TNO1)

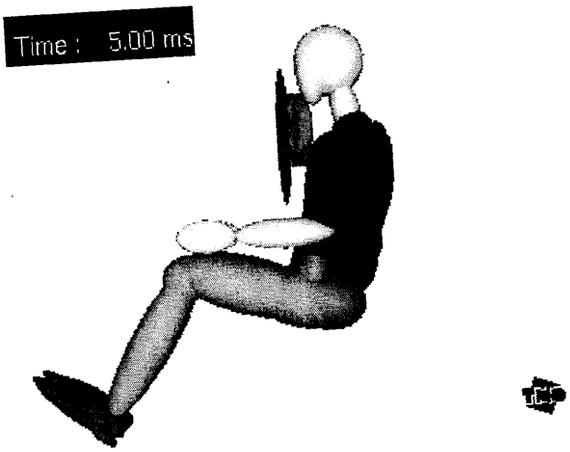

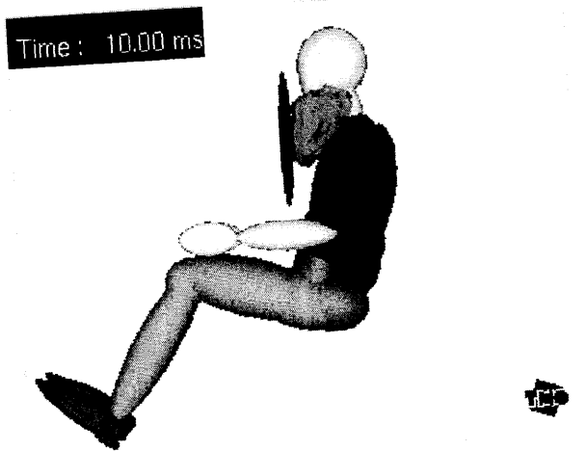

Modified Axial Stiffness (TNO1AX)

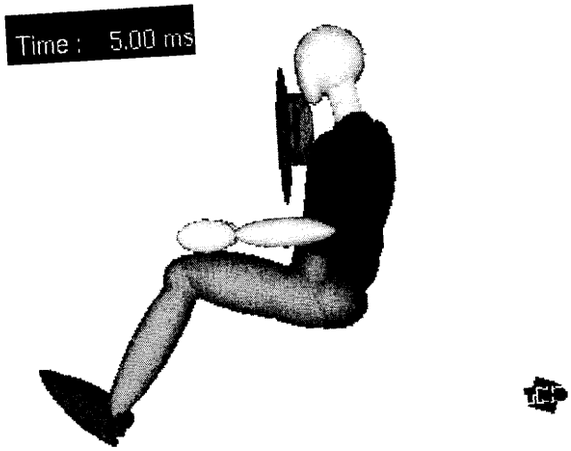

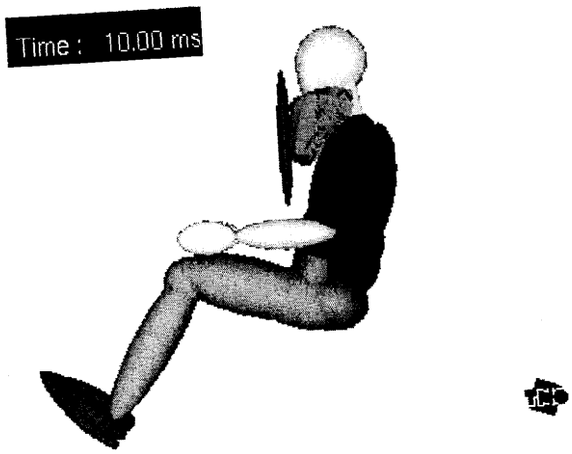

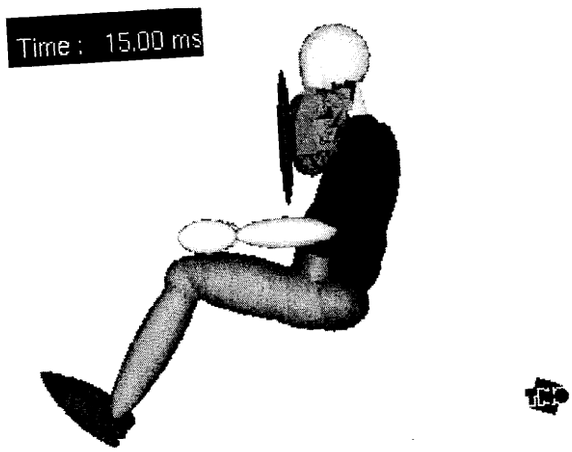

MADYMO Neck (TNO1)

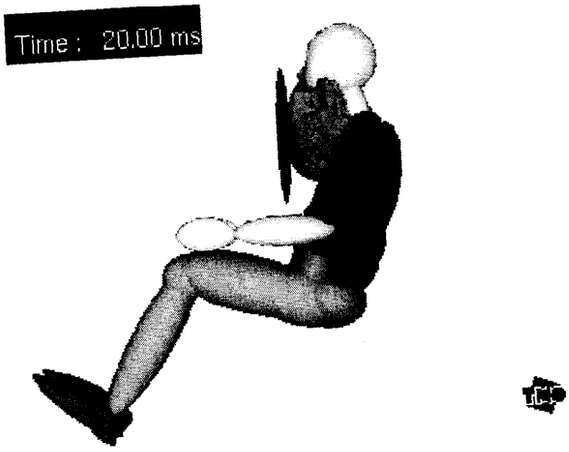

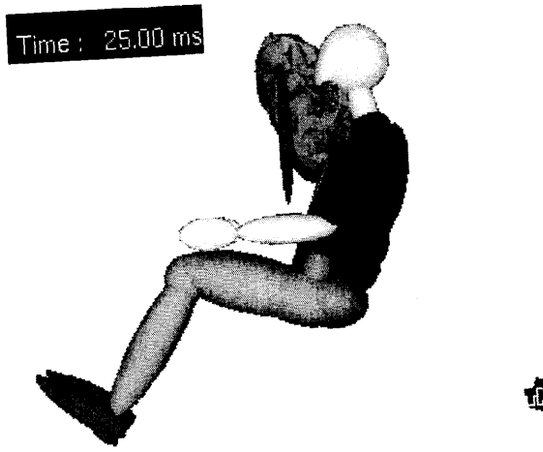

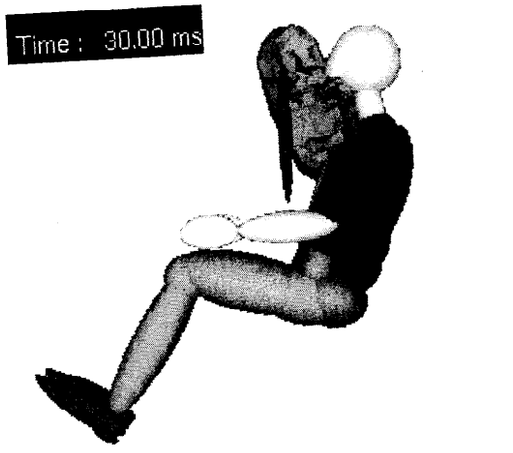

Modified Axial Stiffness (TNO1AX)

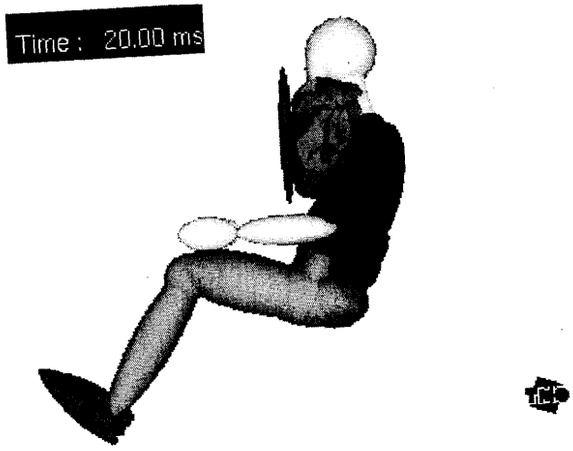

MADYMO Neck (TNO1)

Modified Axial Stiffness (TNO1AX)

MADYMO Neck (TNO1)

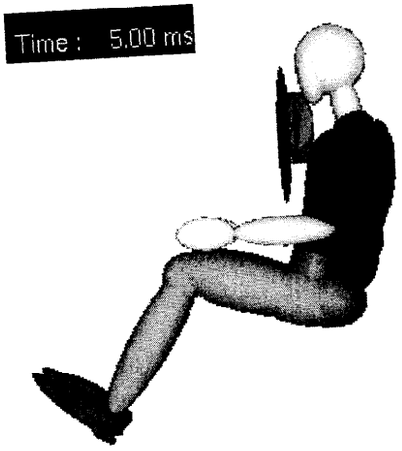

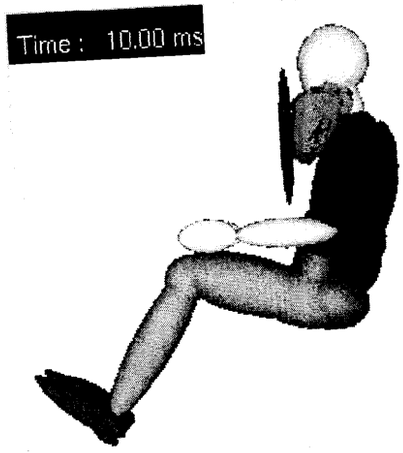

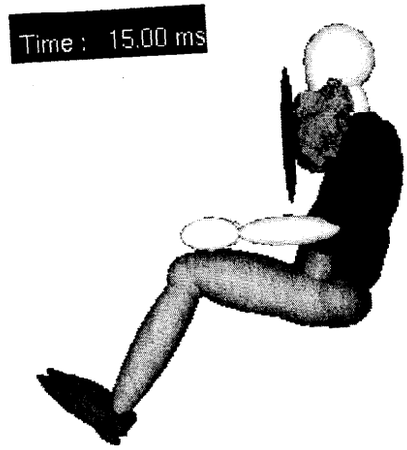

Modified O-C1 and Axial Stiffness (TNO1AXROT)

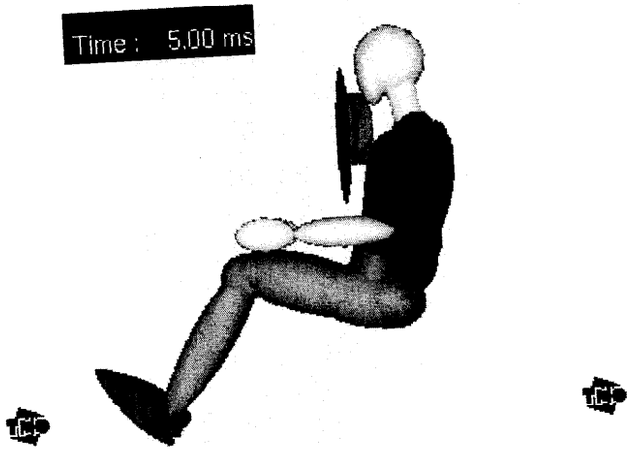

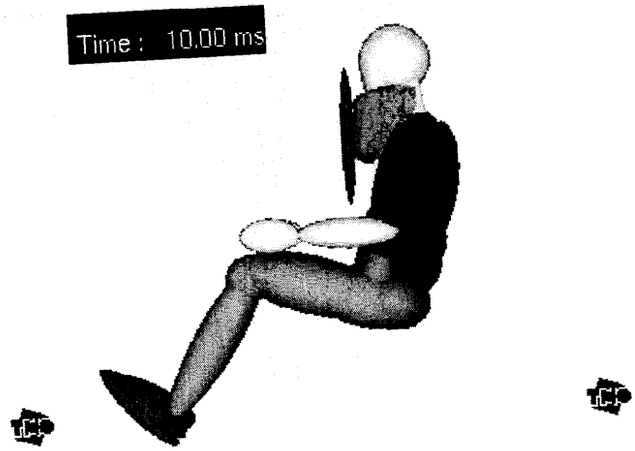

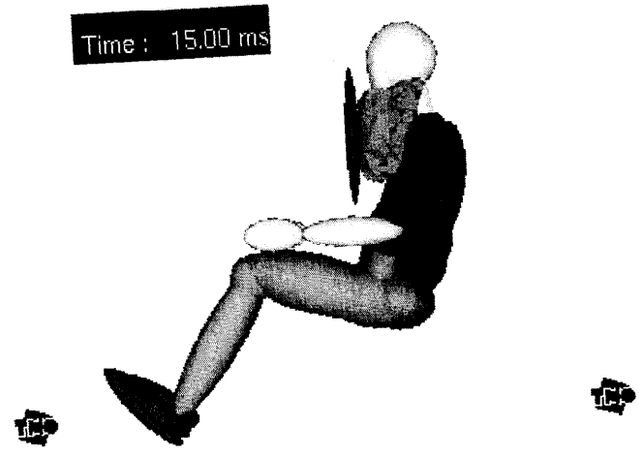

MADYMO Neck (TNO1)

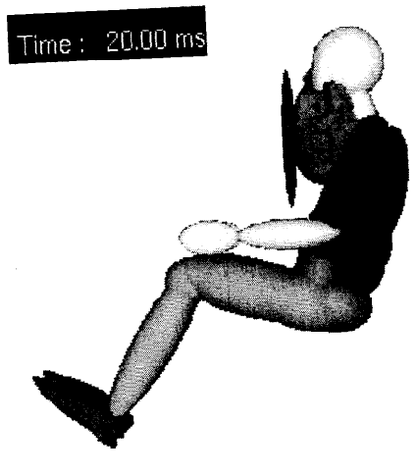

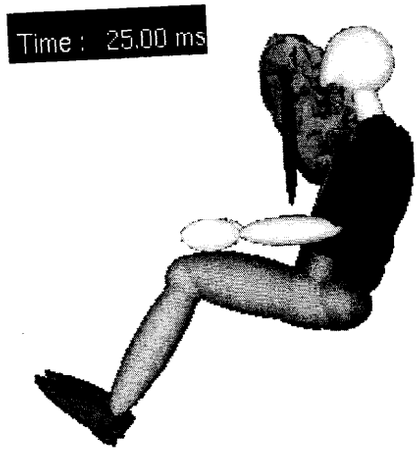

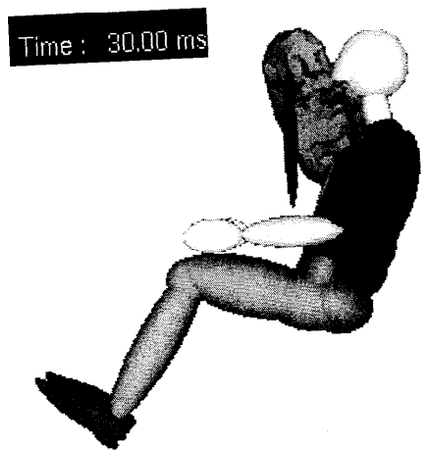

Modified O-C1 and Axial Stiffness (TNO1AXROT)

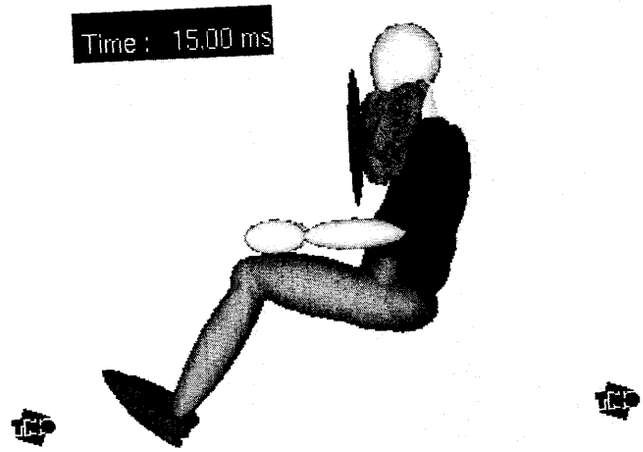

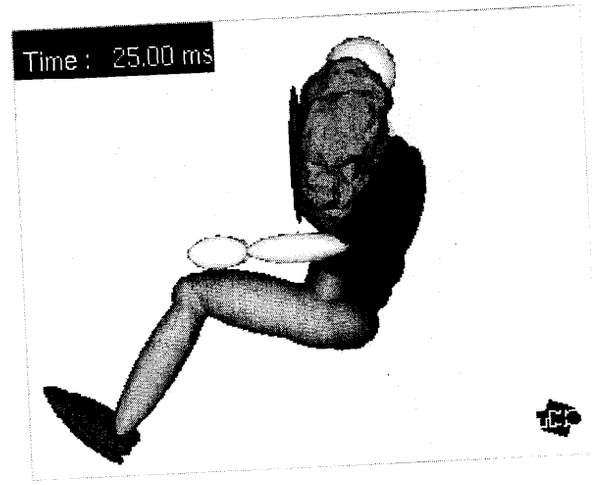

MADYMO Neck (TNO1)

Modified O-C1 and Axial Stiffness (TNO1AXROT)